Thin films of the charge-density-wave oxide $Rb_{0.30}MoO_3$ by pulsed-laser deposition

O. C. Mantel, H. S. J. van der Zant, A. J. Steinfort, and C. Dekker
Department of Applied Physics, Delft University of Technology, Lorentzweg 1, 2628 CJ Delft, The Netherlands

C. Træholt and H. W. Zandbergen
National Centre for HREM, Laboratory of Materials Science, Delft University of Technology, Rotterdamseweg 137, 2628 AL Delft, The Netherlands

(Received 8 July 1996; revised manuscript received 25 October 1996)

Thin films of the model charge-density-wave compound $Rb_{0.30}MoO_3$ (blue bronze) have been grown using pulsed-laser deposition. Films are single-phase $Rb_{0.30}MoO_3$, and consist of grains with typical sizes on the order of micrometers. The charge-density-wave chains are parallel to the film plane. Heteroepitaxial growth of $Rb_{0.30}MoO_3$ is found on $SrTiO_3(100)$ substrates. The blue-bronze grains align their chains with the two principal axes of the square surface lattice of $SrTiO_3(100)$. Preferential orientation into a single direction can be obtained on $SrTiO_3(510)$. Measurements of the film resistance as a function of temperature show a transition to the charge-density-wave state near 182 K. [S0163-1829(97)05407-6]

I. INTRODUCTION

Conductors with a quasi-one-dimensional band structure may exhibit a charge-density-wave (CDW) state below a Peierls temperature T_P.[1,2] Electrons condense into a collective ground state in which the charge density is periodically modulated. If an electric field is applied beyond a certain threshold field, charge is transported by the sliding of the density wave. This CDW transport leads to many interesting phenomena such as, for example, strongly nonlinear conduction, coherent current oscillations, and mode locking at resonant frequencies. Various CDW properties, e.g., the extremely high dielectric constants (up to $\sim 10^8$), are potentially important for applications.

In many ways, CDW's are complementary to superconductors. Properties of CDW's are similar to those of superconductors, with the role of voltage and current interchanged. For example, a dc electric field induces ac current oscillations at a frequency that is proportional to the CDW current density, analogous to the ac Josephson relation for superconductors. Superconducting films have been crucial to fundamental studies on Josephson tunneling and the proximity effect, and have led to important applications such as superconducting quantum interference devices. The CDW counterpart of such phenomena and devices has been unexplored.

To date, CDW's have been studied in bulk crystals only. Thin films of CDW compounds have not been reported yet. The availability of films will open up a new line of research in the field of CDW's. Phase-coherent CDW transport can be studied in (sub)micrometer structures patterned with standard lithography techniques. Combinations of films with normal metals or insulators can be used to fabricate CDW junctions. Recently, first theoretical predictions on mesoscopic CDW systems have been reported.[3–6] Next to the physics of mesoscopic CDW's, thin films will also be important for CDW applications. Any application of a CDW effect in a device will involve thin-film technology.

This paper reports on the growth of thin films of the CDW compound $Rb_{0.30}MoO_3$.[7] The crystal structure of this blue bronze is monoclinic, space group $C2/m$, with lattice parameters $a=18.54$ Å, $b=7.56$ Å, $c=10.04$ Å, and $\beta=118.52°$.[8] The Mo and O atoms form chains of clusters in the [010] direction. These chains are weakly linked to form $(\underline{2}01)$ oriented slabs. The slabs are separated by the rubidium atoms. Because of its anisotropic structure, the resistivity ρ of $Rb_{0.30}MoO_3$ strongly depends on the crystal direction. At room temperature, ρ ranges from about 10^{-3} Ω cm along the chains to about 1 Ω cm perpendicular to the slabs.[9,10] Below the Peierls temperature of 182 K sliding CDW transport is observed along the b axis. $Rb_{0.30}MoO_3$ melts at 560 °C and is one phase in the complex ternary phase diagram of Rb, Mo, and O.[12] As much as 40 binary and ternary Rb-Mo-O compounds have been reported.[13]

We have used pulsed-laser deposition (PLD) for the growth of $Rb_{0.30}MoO_3$ thin films. This technique has been successfully employed for the synthesis of thin films of many materials, in particular, the high-T_c oxide superconductors.[14,15] The PLD setup is described in the next section. Section III contains the experimental results on film growth and characterization. The deposition parameters for the growth of $Rb_{0.30}MoO_3$ are given and the results of different types of analysis are presented. Attention is given to the interaction between substrate and film and to the possibility of growing epitaxial films. In Sec. IV the results on the temperature dependence of the resistance for blue-bronze films are given. In a discussion of the film-growth results (Sec. V), we conclude that the current films are a good starting point for CDW studies on lithographically patterned structures.

II. LASER DEPOSITION SETUP

In a PLD process, the energy of laser pulses is used to ablate material from a target. A film is formed upon transfer of the material to a substrate mounted opposite to this

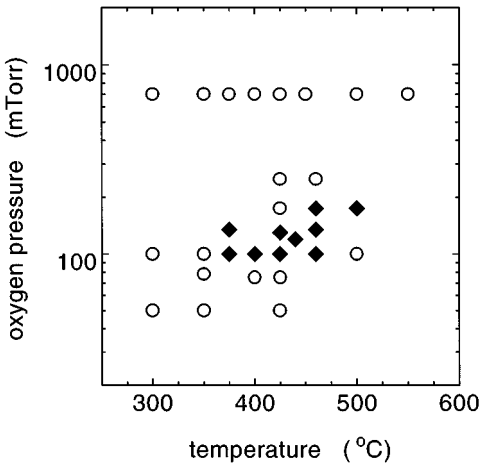

FIG. 1. Film composition in the investigated range of substrate temperatures and oxygen pressures. Solid diamonds represent $Rb_{0.30}MoO_3$ films; open circles indicate films with a different composition. The laser was used at 9 Hz repetition rate and 1.8 J/cm^2 fluence. The films are approximately 1 μm thick.

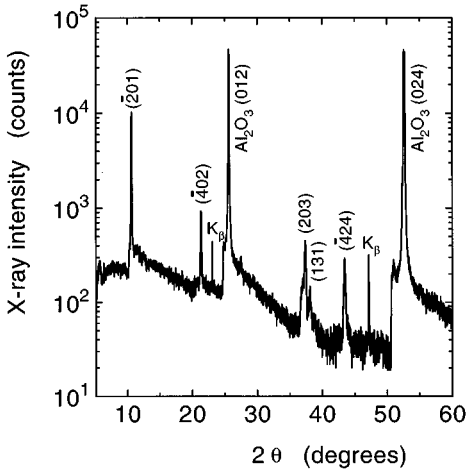

FIG. 2. X-ray spectrum of a $Rb_{0.30}MoO_3$ film grown on an Al_2O_3(012) substrate. The peak at 10.6° is caused by the predominant (201) orientation of the film, for which the CDW chains lie within the plane of the substrate. X-ray wavelength is 1.54 Å (Cu $K\alpha$).

target.[16] We use a Lambda Physik LPX 105E XeCl excimer laser, which produces 20 ns pulses with a wavelength of 308 nm. Pulse energy can be varied between 20 and 150 mJ. By positioning the target slightly out of focus, an approximately 5 mm^2 laser spot size is obtained on the target.

Targets are prepared by pressing a stoichiometric mixture of Rb_2MoO_4, MoO_3, and Mo into pellets. The pellets are heated in an evacuated quartz tube at 530 °C during 36 h. The resulting material is polycrystalline single-phase $Rb_{0.30}MoO_3$, as confirmed by x-ray diffraction (XRD). Targets have a diameter of 21 mm and are typically 3 mm thick.

Substrates ($5\times5\times0.5$ mm^3) are cleaned with organic solvents before mounting on a heater block at 4.7 cm from the target. Typical background pressure of the deposition chamber is 10^{-6} Torr. Oxygen is supplied to the chamber prior to deposition. Deposition times vary between 5 min and 1 h. After deposition, the film is cooled down in the oxygen ambient to below 100 °C (about 30 min) before the chamber is vented with nitrogen. Film thicknesses are determined from measuring the depth profile across a cut through the film with a Tencor Instruments α-step 200 profilometer.

III. RESULTS OF FILM GROWTH

In the PLD process, the composition and structure of films is tuned by the choice of the growth conditions. Important parameters are substrate temperature, oxygen pressure, deposition rate, and the type of substrate used. In this section we present the results from the growth of more than 200 $Rb_{0.30}MoO_3$ films.

A. Film-growth conditions

A series of films was deposited on Al_2O_3(012) (sapphire) at different substrate temperatures and oxygen ambient pressures, keeping all other growth parameters constant. $Rb_{0.30}MoO_3$ films grow at temperatures between 375 °C and 500 °C and at oxygen ambient pressures between 100 and 175 m Torr, as depicted by the solid diamonds in Fig. 1. As a first routine check on the grown phase we check the conductivity and color of the films. $Rb_{0.30}MoO_3$ is conducting and has a dark blue color, which is clearly visible for all the films in this regime. Below 100 m Torr, films consist of a brown-colored amorphous phase, and are electrically conducting. These films have not been further identified. For oxygen pressures higher than 200 m Torr, the grown films are white and insulating. This observation, in combination with XRD and the energy-dispersive analysis of x rays (EDX) results discussed below, suggests that such films consist of a combination of $Rb_2Mo_3O_{10}$ and MoO_3.

XRD was performed on all films. A typical x-ray $\theta-2\theta$ scan of a $Rb_{0.30}MoO_3$ film is shown in Fig. 2. The two largest peaks in the scan are due to the sapphire substrate. Both reflections have a satellite peak as a result of a small Al $K\beta$ wavelength component in the incident radiation. The high peaks at 10.6° and 21.3° are due to the (201) and (402) reflections of $Rb_{0.30}MoO_3$. For (201) and (402) oriented grains the CDW axis (b axis) lies within the film plane. Other peaks in the scan can also be ascribed to $Rb_{0.30}MoO_3$, viz., the (203) and (131) reflections at 37.3° and 38.1° and the (531) reflection at 43.4°. In these orientations the b axis makes an angle with the film plane. No peaks from other phases are found. The strong (201) reflection is a common feature for all $Rb_{0.30}MoO_3$films studied. The occurrence of the other reflections varies from film to film, but those are always at least one order of magnitude weaker than the (201) reflection.

The elemental composition of the series of films grown at 425 °C was determined by EDX at an accelerating voltage of 5 kV and a beam current of 10 nA. Measurements were performed with a spot size of 10 μm diameter at four spots near the corners of the film and at one spot in the middle. The atomic fractions of Rb and Mo in the film were calculated from measured x-ray intensities with a $\phi(\rho z)$ approach.[17] A polycrystalline target consisting of single-phase $Rb_{0.30}MoO_3$ served as a calibration standard. Since the atomic fractions of Rb and Mo do not add up to unity, the

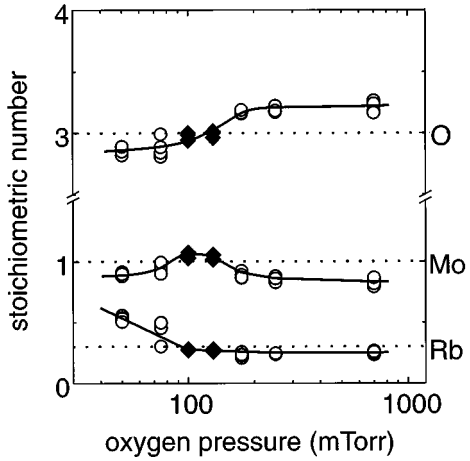

FIG. 3. Results of EDX analysis on a series of films grown at 425 °C on $Al_2O_3(012)$. The solid diamonds represent films that were identified as $Rb_{0.30}MoO_3$ from x-ray analysis and conduction measurements. Solid lines are a guide to the eye. The expected relative amounts of the elements Rb, Mo, and O in $Rb_{0.30}MoO_3$ are indicated by dotted lines.

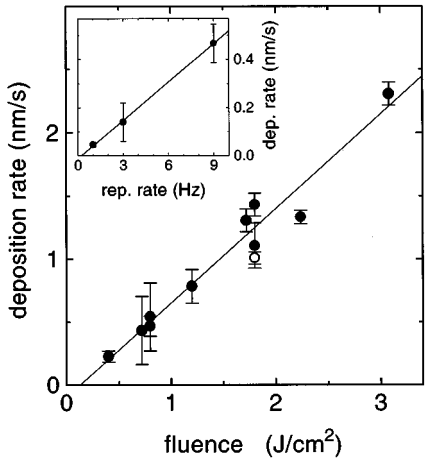

FIG. 4. Film-deposition rate versus laser fluence for films grown on $Al_2O_3(012)$ at a 9 Hz repetition rate. Error bars denote the peak-to-peak film corrugation. Films indicated by solid circles were grown at a temperature of 440 °C and at an oxygen pressure of 120 mTorr. The open circle represents a film grown at 375 °C and 100 m Torr oxygen pressure. The line is a linear fit to the data. The inset shows the dependence of the deposition rate on the pulse-repetition rate, for a fluence of 0.8 nm/s.

remaining fraction can be interpreted as the fraction of oxygen in the films. All fractions are accurate to within 10%.

The atomic fractions of Rb, Mo, and O in the films are plotted versus oxygen pressure in Fig. 3. Data points have been rescaled so that the sum of the three fractions at each oxygen pressure is equal to 4.30, i.e., the number of atoms in the structural formula $Rb_{0.30}MoO_3$. At 100 and 130 m Torr the stoichiometric numbers correspond to the composition $Rb_{0.30}MoO_3$, as expected from the conductivity and color of the films and in agreement with XRD. The Mo concentration is deficient outside the region of pressures where $Rb_{0.30}MoO_3$ is formed. For low oxygen pressure, excess rubidium is found in the films. XRD on such films reveals that at these pressures films are highly amorphous. The oxygen content of films rises monotonically with the oxygen ambient pressure.

B. Variation of the deposition rate

The effect of laser fluence on the film-deposition rate has been investigated by making a series of films at different pulse energies and measuring the resulting film thicknesses (which are between 0.1 and 1.2 μm). The results are shown in Fig. 4. Error bars in the plot denote the peak-to-peak corrugation of the films. Typical deposition rates are found to be of the order of 1 nm/s. In the measured range of fluences, the deposition rate depends linearly on the laser fluence. The deposition rate does not seem to be influenced by the growth temperature (cf. open dot in Fig. 4). In the inset of Fig. 4, the effect of varying the pulse-repetition rate is shown. The deposition rate is proportional to the pulse-repetition rate.

Film composition depends on the deposition rate. For films grown at 470 °C, we find that we no longer grow $Rb_{0.30}MoO_3$ at low repetition rates (3 Hz and lower). An insulating phase is formed instead. From SEM images [see, for example, Fig. 6(b)] we find that blue-bronze films grown with 1 Hz repetition rate at 440 °C contain small white parts which we tentatively ascribe to the same insulating phase.

C. Film morphology

Nine different substrate types were used to investigate the influence of substrate on film morphology. A granular film structure is observed for all substrates. Typically, the grains have an elongated shape. Measurements on the in-plane orientation of the CDW chains, to be discussed in Sec. III D, show that the CDW chains are parallel to the long dimension of a grain. Hence, from morphology studies we can obtain strong indications for in-plane orientation of the CDW chains in a film.

Scanning-electron microscopy (SEM) and x-ray studies show that the (201) grains are randomly oriented on $Al_2O_3(012)$, $LaAlO_3(100)$, $SrLaGaO_4(100)$, $SrLaAlO_4(001)$, and amorphous SiO_2. Some degree of in-plane orientation of grains was found for films grown on $NdGaO_3(110)$. We have focused attention on $SrTiO_3$ substrates. On $SrTiO_3(100)$, $SrTiO_3(110)$, and $SrTiO_3(510)$ grains align with the principal axes of the substrate surface lattice.

Figure 5(a) shows a film grown on $Al_2O_3(012)$ at 440 °C. A dense structure of micrometer-sized elongated grains is observed. These grains are randomly oriented within the film plane. Deposition under similar conditions but at a temperature of 500 °C yields a film with a very different morphology. Figure 5(b) shows an optical-microscopy image. Large elongated grains with sizes of up to 100 μm have formed. These (201) platelets are randomly oriented on the substrate surface. The substrate is visible in between the blue-bronze grains. These are only two examples from a large number of SEM and optical-microscopy images of films on $Al_2O_3(012)$. All such films consist of randomly oriented grains. The size of the grains depends on deposition temperature and ranges from 0.3 μm at 375 °C up to more than 100 μm at 500 °C.

On $SrTiO_3$ substrates we observe alignment of the $Rb_{0.30}MoO_3$ grains with the square lattice of the substrate surface. Films grown on $SrTiO_3(100)$ at 440 °C with a depo-

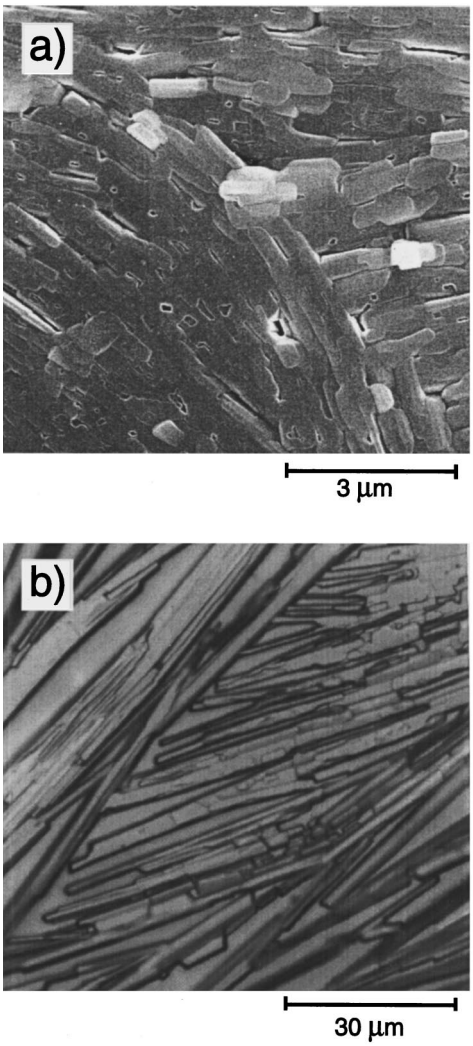

FIG. 5. Morphology of films grown on $Al_2O_3(012)$. (a) SEM image of a film grown at a 440 °C. The deposition rate was 0.5 nm/s. (b) Optical-microscope image of a film grown at 500 °C and a 1.0 nm/s deposition rate.

sition rate of 0.15 nm/s consist of oblongly shaped grains with a length of 1–3 μm and a typical width of 0.2 μm. An example is shown in Fig. 6(a). The grain size is comparable with that of the grains obtained for a film grown on $Al_2O_3(012)$, but now the grains are arranged in two perpendicular directions.

Films grown at lower deposition rates consist of larger grains. Figure 6(b) shows a film grown at a factor of 3 lower repetition rate (1 Hz) than that for the film shown in Fig. 6(a). Oriented elongated grains as long as 30 μm are observed. Note that grain size has increased by one order of magnitude upon lowering the repetition rate from 3 Hz to 1 Hz. The white spots in the SEM image are ascribed to an additional phase in the film as discussed in Sec. III B. The effect of growth temperature on grain size is illustrated by the difference between Figs. 6(b) and 6(c). Grain size decreases by one order of magnitude upon decreasing the temperature from 440 °C [Fig. 6(b)] to 375 °C [Fig. 6(c)].

The corrugation of films decreases with decreasing growth temperature. Surface analysis by atomic-force microscopy shows that films such as shown in Fig. 6(a) have a typical peak-to-peak corrugation of 150 nm, which is quite substantial in view of the average film thickness of 300 nm. At a deposition temperature of 375 °C, the typical corrugation is 50 nm.

From the defined orientation of the substrate edges, we conclude that the grains in films on $SrTiO_3(100)$ are directed with the long dimension along either the [010] or [001] axis of the substrate. At the film-substrate interface, the unit cell of the (201) oriented $Rb_{0.30}MoO_3$surface has dimensions 7.555 Å (b axis) $\times$19.796 Å ([102] direction). The principal axes of the $SrTiO_3(100)$ square surface unit cell both have a lattice mismatch of 3.3% with half the b axis of $Rb_{0.30}MoO_3$. By using the (510) cut of $SrTiO_3$, a predominant orientation into one direction is obtained. The surface unit cell of this substrate is a rectangle of which the long side has a mismatch of 0.6% with the repeat distance in the [102] direction, while the lattice mismatch of the short side (i.e., the c axis of $SrTiO_3$) is the same as for $SrTiO_3(100)$. Figure 6(d) shows a blue-bronze film grown on $SrTiO_3(510)$ at 375 °C. The grains look similar to those grown on $SrTiO_3(100)$ [Fig. 6(c)], but now they are preferentially aligned into one direction.

The alignment of grains with the principal axes of the $SrTiO_3(510)$ substrate surface lattice in $Rb_{0.30}MoO_3$films is suppressed if films are grown at temperatures above 400 °C. For such films, the majority of grains is randomly oriented within the film plane. On $SrTiO_3(110)$ a similar effect is observed: at temperatures below 400 °C grains align into one direction, although less pronounced than for $SrTiO_3(510)$. The alignment does not occur if films are grown at temperatures higher than 400 °C.

D. In-plane orientation of the CDW chains

The in-plane orientation of the CDW chains was investigated by means of an x-ray four-circle diffractometer. Films are aligned such that the ϕ axis of rotation is parallel to the surface normal. A blue-bronze (221) reciprocal vector is then brought into the reflection condition. This vector is a linear combination of the (201) vector, parallel to the axis of rotation, and the $Rb_{0.30}MoO_3(010)$ vector. By rotation over ϕ, a scan is made over all possible orientations of the $Rb_{0.30}MoO_3$ b axis within the film plane. In a similar way the orientations of the principal axes of the $SrTiO_3$ surface lattice are determined.

Figure 7(a) shows the result of such an analysis on the film of Fig. 6(a). The b axes of the $Rb_{0.30}MoO_3(201)$ grains appear to lie parallel to the principal axes of the $SrTiO_3$ substrate. The interaction between substrate and film is thus confirmed. The $Rb_{0.30}MoO_3$ reflections have a full width at half maximum (FWHM) of about 2°, which is ascribed to a mosaic spread due to an orientation distribution of the grains.

A similar measurement was performed on a film grown on $SrTiO_3(510)$ at 375 °C [Fig. 7(b)]. The observed peaks in the ϕ scan again confirm an in-plane orientation of the CDW chains. The b axis is predominantly oriented into one direction, as is shown by the difference in intensity between the reflections. After determination of the principal axes of the substrate surface, we find that the majority of the (201) grains has the b axis aligned with the [001] axis of the

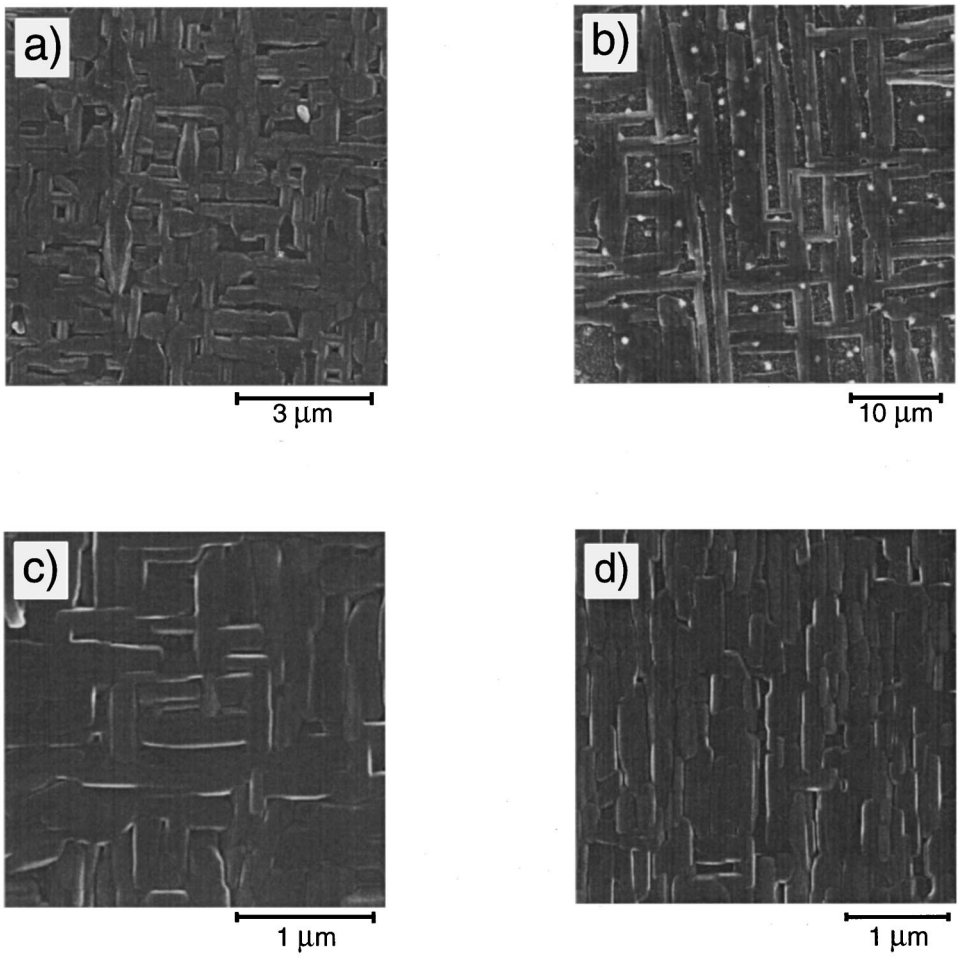

FIG. 6. SEM analysis of films grown on $SrTiO_3$. (a) film grown on $SrTiO_3(100)$ at 440 °C and a 0.15 nm/s deposition rate. (b) Similar film, grown at a 0.05 nm/s deposition rate. (c) film grown on $SrTiO_3(100)$ at a 0.05 nm/s repetition rate, but at a lower temperature (375 °C). (d) film grown on $SrTiO_3(510)$ at 375 °C and a 0.15 nm/s deposition rate.

$SrTiO_3(510)$ substrate. These grains cause the high reflections at $-138°$ and 42°. The smaller peaks at $-48°$ and 132° are due to grains for which the *b* axis is directed along the $[\underline{1}50]$ direction of $SrTiO_3$. The FWHM of the high reflections is approximately 2°.

The in-plane orientation of the CDW chains in a film grown on $SrTiO_3(510)$ at 440 °C was measured in a similar way. A ϕ scan shows that only a few percent of the chains is aligned parallel to the [001] axis of the substrate. The rest of the film has a random orientation within the film plane, in accordance with SEM images of similar films that show a suppressed alignment of grains on $SrTiO_3(510)$ at a growth temperature of 440 °C (see Sec. III C). Measurements such as those shown in Fig. 7(b) can be used to determine the direction of the CDW chains within a grain. The x-ray data reveal the in-plane orientation of the CDW chains, whereas a SEM image of the same film shows the orientation of grains. It turns out that the majority of *b* axes is aligned parallel to the direction along which the long dimension of most of the grains is directed. Thus, we find that the CDW chains in a single grain lie along its long dimension, in agreement with results from transmission-electron microscopy (TEM) analysis on a single grain.[18] For substrates on which the grain orientation is random, no predominant in-plane orientation of the CDW chains was found. ϕ scans of films grown on $Al_2O_3(012)$, $LaAlO_3(100)$, $SrLaGaO_4(100)$, and $SrLaAlO_4(001)$ show an x-ray signal that is independent of ϕ.

E. Film-substrate interface

The interface between film and substrate has been studied with cross-sectional TEM. For all films, preparation for TEM proved difficult because of the poor adhesion to the substrate.

Figure 8 shows the interface for a blue-bronze film grown on $Al_2O_3(012)$. In the upper part, unit cells of the film are visible. The lower part shows the lattice fringes of the substrate. Film and substrate are separated by an amorphous layer with a thickness of 24 nm. Using the known spacing of the substrate planes (3.48 Å) as a calibration, we find a spacing of 8.3 ± 0.2 Å between lattice planes in the $Rb_{0.30}MoO_3$ film. This is in agreement with the expected value of 8.3 Å for the distance between $(\underline{2}01)$ planes. In the $Rb_{0.30}MoO_3$ film, fringes from the $(\underline{1}11)$ and $(\underline{1}10)$ planes are visible at angles of 58° and 76° with the $(\underline{2}01)$ planes, respectively. EDX element analysis on the interface layer shows that its chemical composition is AlO_x. Since the layer has an equal thickness everywhere on the sample it is concluded that it is not an artifact of the TEM preparation. The origin of the formation of the interface layer is not understood. Reflection high-energy-electron diffraction measurements on a bare substrate show that it is not present prior to deposition.

Figure 9 is a TEM image of a $SrTiO_3(100)$-$Rb_{0.30}MoO_3$ interface. A sharp interface between substrate and film is observed. In this case, no interface layer is found. Using the distance of 3.91 Å between substrate planes as an internal

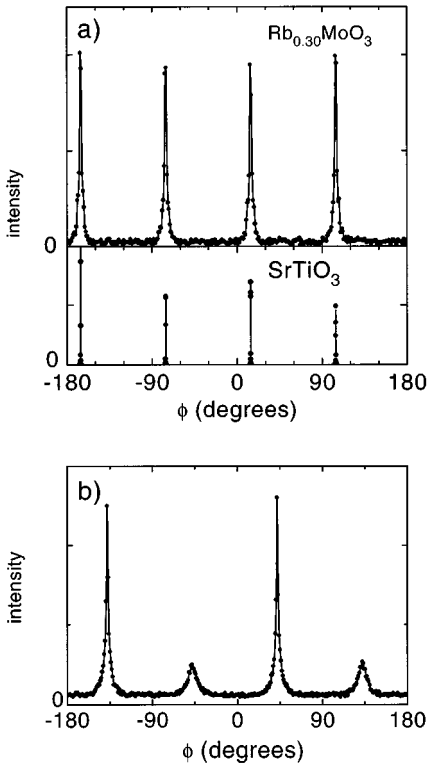

FIG. 7. (a) Intensity of the blue-bronze $(\bar{2}21)$ reflection (top) and the $SrTiO_3$ (220), (202), (220), and $(20\bar{2})$ reflections (bottom) as a function of azimuthal angle ϕ. The figure shows that the directions of the CDW chains in the film grains are parallel to the principal axes of the substrate surface lattice. (b) Intensity of the blue-bronze $(\bar{2}21)$ reflection as a function of the azimuthal angle ϕ for a film grown on $SrTiO_3(510)$. The two high reflections are caused by grains that have the CDW chains aligned with the *c* axis of the substrate.

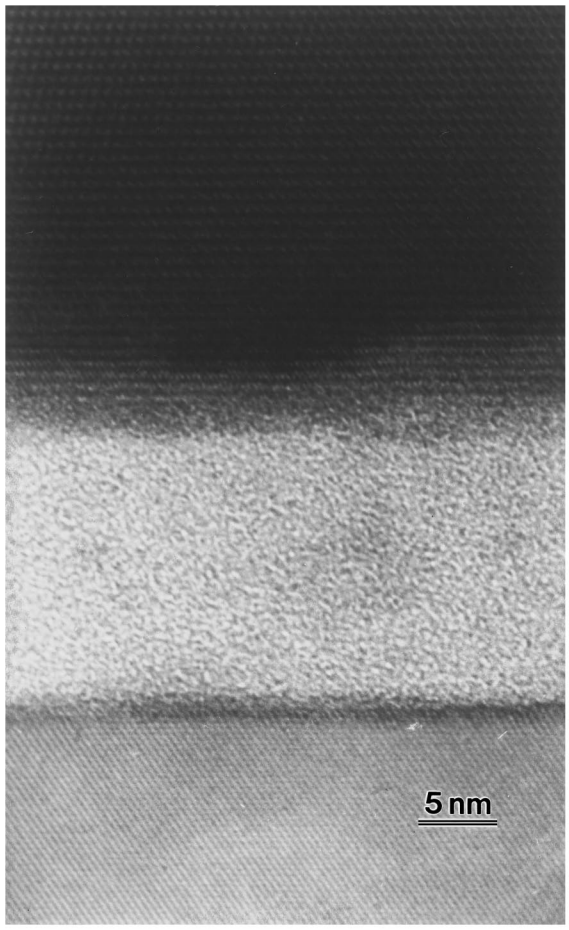

FIG. 8. High-resolution TEM image of a film grown on $Al_2O_3(012)$ with a deposition rate of 1.4 nm/s at 425 °C and at 110 m Torr oxygen pressure. At the $Al_2O_3(012)$ interface an amorphous layer of 24 nm thickness is present.

calibration, the spacing between lattice planes in the film is found to be 8.4 ± 0.2 Å. These lattice planes can thus be identified as $(20\bar{1})$ $Rb_{0.30}MoO_3$ planes. No other lattice fringes are visible in the film. The sharp interface confirms heteroepitaxial growth of the film on the substrate. The interaction between film and substrate results in the observed alignment of film grains, with the CDW chains of blue bronze parallel to the substrate principal axes (Secs. III C and III D).

IV. ELECTRICAL TRANSPORT

We have determined the Peierls temperature and the CDW energy gap for blue-bronze films from measurements of the low-bias resistivity as a function of temperature. Experiments have been performed for several films and one crystal in a helium-flow cryostat. On the films, gold contacts of 100×200 μm^2 were evaporated with a spacing of 500 μm. Wires were attached by ultrasonic bonding. Data are compared with measurements on a blue-bronze crystal, for which current contacts were 1 mm apart. Resistivities are calculated from the sample geometry.

Figure 10 shows the resistivity as a function of temperature for a typical film and for the crystal. For both, a sharp increase of the resistivity below 182 K is observed, consistent with the opening of a gap at the Peierls temperature. In the inset the behavior of the resistivity near the Peierls transition is demonstrated. The transition temperature of the crystal is deduced from the dip in $d\ln(\rho)/dT$ and is equal to 182 K. For the film, the curve merely shows a kink near 182 K.

In the low-temperature regime, a good fit to the data is obtained if the temperature dependence of the Peierls gap is taken according to the BCS model. Both experimental curves are consistent with a fit of $\rho(T)\propto\exp[\Delta(T)/k_BT]$, with $\Delta(T)$ the temperature-dependent Peierls gap. We find a zero-temperature gap of $\Delta(0)=470$ K for the film and $\Delta(0)=530$ K for the crystal, in agreement with typical values of 500 K that have been reported in the literature.[11,19,20] The results on films seem to indicate that the zero-temperature energy gap depends on grain size. Films that consist of smaller grains have a $\Delta(0)$ that is somewhat suppressed as compared to the bulk value.

At room temperature, the resistivities of film and crystal are of the same order of magnitude. However, their temperature dependence above the Peierls temperature is different. Unlike the crystal, which shows metallic behavior, the resistivity of the film increases with decreasing temperature. This effect is ascribed to the granular nature of the films.

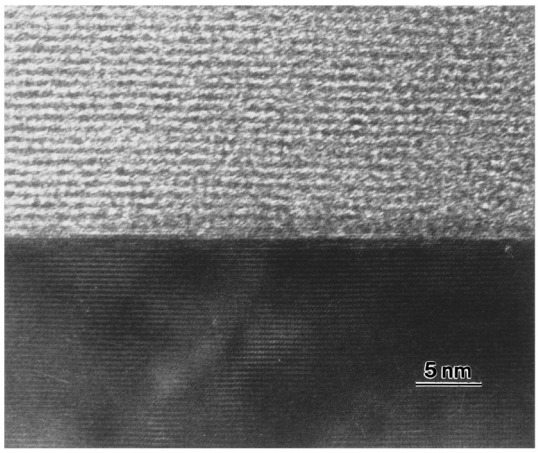

FIG. 9. High-resolution TEM image of a film grown on $SrTiO_3(100)$. Growth conditions are a deposition rate of 1.4 nm/s, a temperature of 440 °C , and 120 m Torr oxygen pressure. A sharp film-substrate interface is observed.

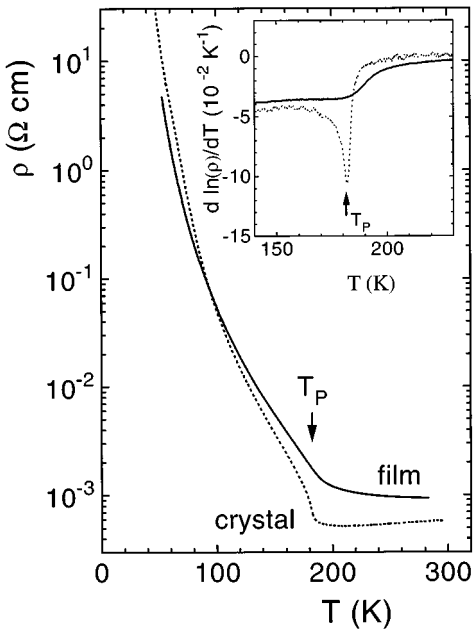

FIG. 10. Resistivity versus temperature of a $Rb_{0.30}MoO_3$ film (solid line) and crystal (dotted line). The inset shows the same data plotted as $d\ln(\rho)/dT$ versus T, demonstrating the behavior near the Peierls transition. Growth conditions are an $Al_2O_3(012)$ substrate temperature of 460 °C, an oxygen pressure of 150 m Torr, and a 1.4 nm/s deposition rate. The film thickness is 1 μm.

V. DISCUSSION

The present films serve as a starting point for the study of charge-density-wave transport at a (sub)micrometer scale. Films will be patterned by the use of lithographic techniques, resulting in a well-defined measurement geometry. Here, we discuss compositional and morphological aspects of the film growth that seem relevant for future electrical-transport measurements.

The growth parameters for the deposition of $Rb_{0.30}MoO_3$ films appear to be quite critical. Single-phase $Rb_{0.30}MoO_3$ films can only be grown for a narrow range of oxygen pressures (100–175 m Torr). The temperature range for growth ($\sim$375–500 °C) is shifted to lower values upon a decrease of the deposition rate. The used substrate type does not seem to affect the range of substrate temperatures and oxygen pressures at which $Rb_{0.30}MoO_3$ is formed. Thermodynamic studies on bulk systems of the elements Rb, Mo, and O show that $Rb_{0.30}MoO_3$ is formed only in a narrow region of the ternary phase diagram,[12] which is in line with the observed critical dependence of the film composition on growth parameters.

The granular structure of the $Rb_{0.30}MoO_3$ films indicates that island growth occurs rather than layer-by-layer growth. The size of the grains depends on the deposition rate and substrate temperature during growth. The largest grains are grown at high temperatures and at low deposition rates. This suggests that the grain size is determined by the mobility of the deposited material on the substrate surface. AFM studies on the initial stage of blue-bronze film growth show that three-dimensional islands as high as 50 nm are formed on the bare substrate surface.[21]

Phase-coherent CDW transport may be measured if one grain can be contacted and if the distance between the contacts is smaller than the CDW phase-coherence length. This length is likely to be in the micrometer range along the CDW chains for typical bulk blue-bronze samples.[22] For most films, the long dimension of the grains, which is parallel to the CDW chains, has a length of typically 1 μm. Therefore, (sub)micrometer patterning on the current films will allow us to enter the regime of phase-coherent CDW transport. Note that not only the size of the grains has to be taken into account in considerations of phase-coherent transport measurements. Random orientation of the CDW chains within the film plane as well as a large surface corrugation can make films less suitable for lithographic patterning.

Alignment of grains within the plane of the film is important because of the quasi-one-dimensional structure of $Rb_{0.30}MoO_3$. Since CDW transport only occurs along the *b* axis, it is desirable for electrical transport measurements that all grains have this axis oriented into the same direction. While the *b* axis always lies within the film plane, orientation is random within this plane for most substrate types studied. In-plane alignment has been found on $SrTiO_3$. On $SrTiO_3(100)$ and $SrTiO_3(510)$ grains can be aligned into two and one direction, respectively, coinciding with the principal axes of the substrate surface lattice.

Because larger grains are grown at higher deposition temperatures, a logical step would be to grow films on $SrTiO_3(510)$ and $SrTiO_3(110)$ at high deposition temperatures (440 °C, for example). However, we find that the alignment of grains within the film plane is suppressed for such films. This suppression of in-plane orientation at elevated growth temperatures is not yet understood.

Electrical transport data on $Rb_{0.30}MoO_3$ films with 0.5 mm spaced contacts show a Peierls transition near 182 K. This transition is smeared out over several kelvin for all the films studied. The energy gap below the Peierls transition is somewhat reduced as compared to bulk-crystal values. The results indicate that the electrical-transport properties depend

on the morphology of the films. A more systematic study is needed for a quantitative comparison between films.

The in-plane oriented $Rb_{0.30}MoO_3$ films on $SrTiO_3$ are a good starting point for the study of the mesoscopic aspects of charge-density waves. (Sub)micrometer structures can be defined on the films by lateral lithographic patterning.[23] Such well-defined samples allow the investigation of different CDW phenomena such as, for example, phase-coherent transport, proximity effects, and size effects.

ACKNOWLEDGMENTS

We wish to acknowledge Hans Mooij, Vladimir Matijasevic, Mark Visscher, Behzad Rejaei, and Gerrit Bauer for discussions, Leo Lander for technical assistance, J. Marcus for discussions on target preparation, and D. van der Marel for supplying the $SrLaGaO_4(100)$ and $SrLaAlO_4(001)$ substrates. This work was supported by the Netherlands Foundation for Fundamental Research on Matter (FOM).

[1] G. Grüner, *Density Waves in Solids* (Addison-Wesley, Reading, MA, 1994).
[2] P. Monceau, in *Electronic Properties of Quasi-One-Dimensional Metals*, edited by P. Monceau (Reidel, Dordrecht, 1985), Vol. 2.
[3] M. I. Visscher and G. E. W. Bauer, Phys. Rev. B **54**, 2798 (1996).
[4] M. I. Visscher, B. Rejaei, and G. E. W. Bauer, Europhys. Lett. (to be published).
[5] B. Rejaei and G. E. W. Bauer, Phys. Rev. B **54**, 8487 (1996).
[6] Y. Tanaka, M. I. Visscher, B. Rejaei, and G. E. W. Bauer, Solid State Commun. **100**, 37 (1996).
[7] H. S. J. van der Zant, O. C. Mantel, C. Dekker, J. E. Mooij, and C. Træholt, Appl. Phys. Lett. **68**, 3823 (1996).
[8] W. J. Schutte and J. L. de Boer, Acta Crystallogr. Sec. B **49**, 579 (1993).
[9] E. Bervas, Thèse d'Ingénieur-Docteur, Université de Grenoble, 1984.
[10] Wang Xue-Mei, Zhang Dian-lin, and Zhang Yuheng, Phys. Rev. B **45**, 13 250 (1992).
[11] C. Schlenker, J. Dumas, C. Escribe-Filippini, and H. Guyot, in *Low-Dimensional Electronic Properties of Molybdenum Bronzes and Oxides*, edited by C. Schlenker (Kluwer, Norwell, MA, 1989), pp. 159–257.
[12] J. Reau, C. Fouassier, and P. Hagenmuller, J. Solid State Chem. **1**, 326 (1970).
[13] *JCPDS Powder Diffraction File* (International Centre for Diffraction Data, Swarthmore, 1991).
[14] *Pulsed Laser Deposition of Thin Films*, edited by D. B. Chrisey and G. K. Hubler (Wiley, New York, 1994).
[15] T. Venkatesan *et al.*, Appl. Phys. Lett. **54**, 581 (1989).
[16] N. Y. Chen, Ph. D. thesis, Delft University of Technology, 1995.
[17] See, for example, V. D. Scott, G. Love and S. J. B. Reed, *Quantitative Electron-Probe Microanalysis* (Horwood, New York, 1995).
[18] O. C. Mantel, H. S. J. van der Zant, A. J. Steinfort, C. Træholt, and C. Dekker, Synth. Met. (to be published).
[19] W. Brütting, P. H. Nguyen, W. Rieß, and G. Paasch, Phys. Rev. B **51**, 9533 (1995).
[20] Tae Wan Kim, D. Reagor, G. Grüner, K. Maki, and A. Virosztek, Phys. Rev. B **40**, 5372 (1989).
[21] H. S. J. van der Zant, O. C. Mantel, and C. Dekker (unpublished).
[22] S. M. DeLand, G. Mozurkewich, and L. D. Chapman, Phys. Rev. Lett. **66**, 2026 (1991).
[23] H. S. J. van der Zant, O. C. Mantel, C. P. Heij, and C. Dekker, Synth. Met. (to be published).